International Journal of Heat and Mass Transfer 123 (2018) 137–142

Contents lists available at ScienceDirect

International Journal of Heat and Mass Transfer

journal homepage: www.elsevier.com/locate/ijhmt

A simple efficient method of nanofilm-on-bulk-substrate thermal conductivity measurement using Raman thermometry

Vladimir Poborchii [a,*], Noriyuki Uchida [a], Yoshinobu Miyazaki [a], Tetsuya Tada [a], Pavel I. Geshev [b,c], Zhandos N. Utegulov [d], Alexey Volkov [e]

[a] Nanoelectronics Research Institute, National Institute of Advanced Industrial Science and Technology, 1-1-1 Higashi, AIST Central-5, Tsukuba 305-8565, Japan
[b] Institute of Thermophysics of the Russian Academy of Sciences, Lavrentyev Ave. 1, Russia
[c] Novosibirsk State University, Pirogova Str. 2, Novosibirsk 630090, Russia
[d] Department of Physics, School of Science and Technology, Nazarbayev University, 53 Kabanbai Batyr Ave., Astana 010000, Kazakhstan
[e] Interdisciplinary Instrumentation Center, National Laboratory Astana, Nazarbayev University, 53 Kabanbai Batyr Ave., Astana 010000, Kazakhstan

ARTICLE INFO

Article history:
Received 16 October 2017
Received in revised form 17 February 2018
Accepted 19 February 2018
Available online 20 March 2018

ABSTRACT

In contrast to known Raman-thermometric measurements of thermal conductivity (k) of suspended Si nano-membranes, here we apply Raman thermometry for k measurement of mono- and nano-crystalline Si films on quartz, which is important for applications in thermoelectricity and nanoelectronics. Experimentally, we measure linear dependence of the laser-induced Raman band downshift, which is proportional to the moderate heating ΔT, on the laser power P. Then we convert the downshift to ΔT and determine the ratio $\Delta T/P$. The actual power absorbed by the film is calculated theoretically and controlled experimentally by the reflection/transmission measurement. Then we calculate $\Delta T_{calc}/P$ for arbitrary film k assuming diffusive phonon transport (DPT). Film k is determined from the condition $\Delta T/P = \Delta T_{calc}/P$. We show that this method works well for films with thickness $h > \Lambda$, where Λ is phonon-mean-free path, even for low-k films like nano-crystalline Si and SiGe. For $h < \Lambda$, despite ballistic phonon transport contribution, this approach works when the in-plane DPT dominates, e.g. in Si films on quartz with $h \geq 60$ nm. We also show that the influence of thermal boundary resistance on the determined k is negligible at this condition. The proposed method is simple and time efficient, as dozen of films can be examined in one hour.

1. Introduction

Measurement of thermal conductivity (k) of nanofilms (NFs) and, especially, Si-based NFs is important for applications in thermoelectricity and nanoelectronics. NF k is reduced compared to bulk material due to phonon boundary scattering and some other effects. Reduced k limits the ability to remove waste heat in microprocessors, light-emitting diodes, memory and solar-cell devices. On the other hand, a reduced k can play a positive role in thermoelectric devices. The efficiency of such devices depends on the thermoelectric figure of merit $ZT = S^2T\sigma/k$, where S, σ and T are the Seebeck coefficient, electrical conductivity, and absolute temperature of material, respectively. Bulk Si was never used in thermoelectric applications due to its high $k \sim 150$ W/m/K and, therefore, low ZT < 0.01 at room temperature. Although Si is a poor thermoelectric material, a reduction of k in Si NFs and nanowires (NWs) can considerably improve their performance [1–9]. Further k reduction can be achieved in nanocrystalline Si-based NFs [10,11]. In the composites consisting of Si and Ni silicide nanocrystals (Ni-Si NC), due to both phonon scattering at the grain boundaries and planar defects, the films have much lower k (3–7.7 W/m/K) and higher ZT (>0.1) than bulk Si at room temperature [11].

Among a variety of methods of k measurements of Si-based nanostructures, non-contact Raman thermometry is, especially, attractive. At moderate laser-induced heating ΔT, Si optical phonon ~520.5 cm^{-1} Raman band displays downshift $\Delta\omega$ (cm^{-1}) = $-0.022\Delta T$ (K) [12]. For unsupported Si particles, overheating can be substantial, i.e. $\Delta T > 1000$ K is possible at rather low laser power $P \sim 1$ mW since there is no efficient heat drain [13]. Contrary, in bulk materials and suspended or supported nanostructures, there is a heat drain. If we correctly take the drain into account then we can extract k from the Raman thermometric data.

Recently, Raman thermometry was utilized to measure k in bulk absorbing materials [14,15], suspended nano-membranes [14,16–22] (NMs) and NWs [23–26]. Even time-domain differential Raman thermometry was developed in recent experiments [27]. The ΔT of the illuminated NM/NW area depends on the k,

* Corresponding author.
E-mail address: Vladimir.p@aist.go.jp (V. Poborchii).

https://doi.org/10.1016/j.ijheatmasstransfer.2018.02.074
0017-9310/

absorption of NM/NW, P, laser beam diameter and the distance of the area from the heat drain. Since the k is the only unknown parameter, one can find it. For ultrathin suspended NMs, ambient environment detrimentally affect ΔT, which is a disadvantage of the Raman thermometry in this case as was shown for grapheme [18].

In contrast to suspended NMs and NWs, here we consider NFs on bulk substrates, in which the effect of ambient environment is much less than that for suspended NMs/NWs. The dominant heat drain is a few millimeter thick substrate supporting NF. Therefore, the experimental Raman measurement procedure is very simple, just standard micro-Raman spectra acquisition. However, the k extraction from ΔT is rather complicated in this case. We solve this problem for absorbing NF on bulk non-absorbing low-k substrate and measure k of Si NFs and composite NC NFs of Si and Fe silicide (Fe-Si NC) NFs on quartz. Fe-Si NC is similar to Ni-Si NC but more advantageous for industrial fabrication due to its lower cost. Additionally, we fabricated NC SiGe film and showed further decrease in the thermal conductivity due to the enhancement of the alloy phonon scattering. Our presented method for k measurement for NF-on-substrate is simpler and more efficient than alternative methods. A dozen of NFs can be examined in one hour.

2. Theoretical calculation of the laser-induced heating of absorbing nanofilm on transparent bulk substrate

As shown in Fig. 1a, we consider an absorbing layer 1 with complex refractive index $N_1 = \sqrt{\varepsilon_1} = n_1 + i\kappa_1$ and thickness h ($0 \le z \le h$) on a semi-infinite substrate (layer 2) with the refractive index $N_2 = \sqrt{\varepsilon_2} = n_2$ ($z > h$). Laser light propagates from a semi-infinite media with the refractive index $N_0 = \sqrt{\varepsilon_0} = n_0$ ($z < 0$), hits the absorbing layer 1 and propagates further into the layer 2. The laser-light-power-flux density is:

$$S = (P/\pi r_0^2)\exp(-r^2/r_0^2), \tag{1}$$

where r_0 is the radius of the focused laser beam (Fig. 1a, b). The volume density of heat per second generated by the light absorption can be expressed as follows [28]:

$$q_V = \varepsilon_1''|E_1|^2\omega/(8\pi) \tag{2}$$

where ω is the light frequency, ε_1'' is the imaginary part of dielectric constant and E_1 is the electric field of light in the layer 1. We calculate E_0, E_1 and E_2 using exact analytical solution of Maxwell equations for layered medium taking into account reflection, absorption and interference [29]. Fig. 2a shows functions $q_V(z)$ for 75 nm thick Si on quartz (SOQ) at the center of the laser beam ($x = 0$, $r_0 = 250$ nm) for the wavelength $\lambda = 561$ nm ($n_1 = 4.05, \kappa_1 = 0.035$) and for $\lambda = 364$ nm ($n_1 = 6.45, \kappa_1 = 2.76$). The 364 nm light is nearly completely absorbed in ~20 nm thick layer with no noticeable interference while the 561 nm light displays interference. At $\lambda = 561$ nm, the SOQ absorption A is ~7.4% with reflection $R \sim 16.1\%$ and transmission $Tr \sim 76.5\%$.

For experimental control of the film A, we measured reflection/transmission spectra. Then we determined A from $A = 100\% - R - Tr$. Fig. 3 shows experimental and theoretical reflection spectra of 59 nm and 64 nm thick SOQ. The agreement between experiment and theory is very good. Statistically, we estimated that the

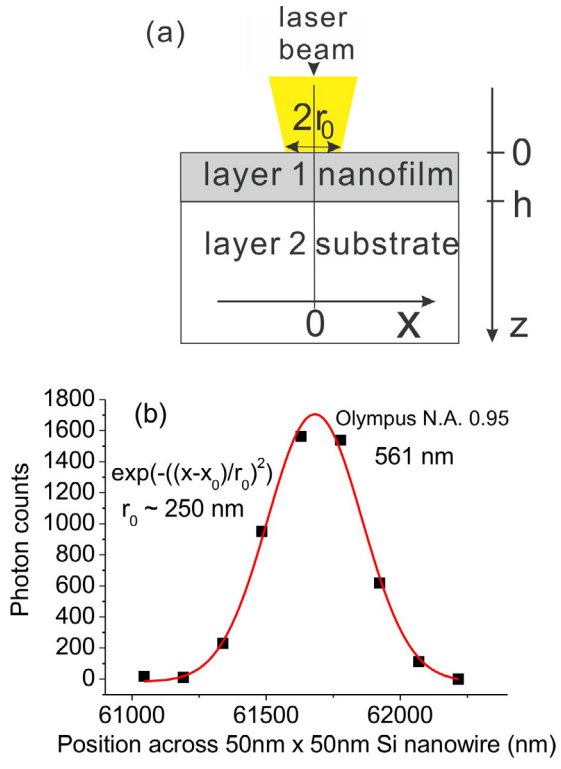

Fig. 1. (a) Schematic view of laser illumination of absorbing NF on transparent substrate; (b) light intensity distribution in the focused 561 nm laser beam measured while scanning the beam across 50 nm × 50 nm Si NW and detecting NW Raman signal (black squares). Red curve shows Gaussian fitting of the experimental points. (For interpretation of the references to color in this figure legend, the reader is referred to the web version of this article.)

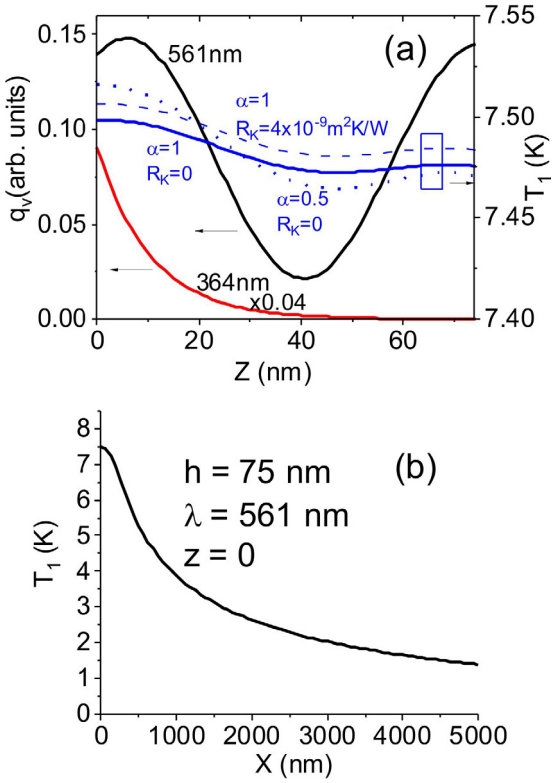

Fig. 2. (a) The volume density of heat per second $q_V(z)$ at $x = 0$ generated in 75 nm thick SOQ by the 561 nm (black curve) and 364 nm (red curve) absorbed light ($r_0 = 250$ nm) correspond to the left axis; the temperature (heating) field $T_1(z)$ for the 561 nm light with $P = 1$ mW for three cases (blue curves): (1) no anisotropy of the film thermal conductivity $\alpha = 1$ and no Kapitza resistance $R_K = 0$ (solid); 2) $\alpha = 1$ and $R_K = 4 \times 10^{-9}$ m^2 K/W (dashed); (3) $\alpha = 0.5$ and $R_K = 0$ (dotted) correspond to the right axis; (b) temperature (heating) field $T_1(x)$ at $z = 0$ for 75 nm thick SOQ. The $T_1(x)$ curves corresponding to three cases with different α and R_K shown in (a) cannot be distinguished in this scale. (For interpretation of the references to color in this figure legend, the reader is referred to the web version of this article.)

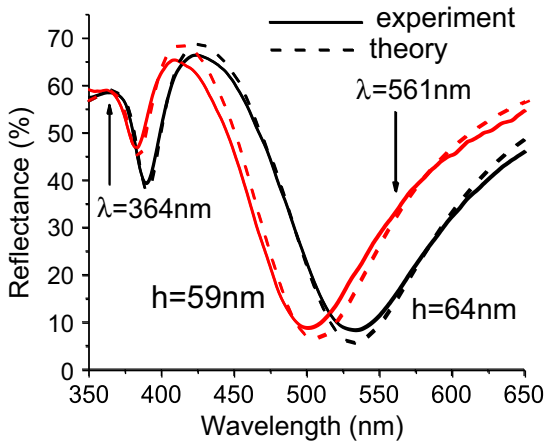

Fig. 3. Experimental (solid lines) and theoretical (dashed lines) reflection spectra of 59 nm (red) and 64 nm (black) thick SOQ NFs. (For interpretation of the references to color in this figure legend, the reader is referred to the web version of this article.)

discrepancy between experimentally and theoretically determined film absorption was <10%.

We need to solve the stationary heat transfer problem for a layered medium with the laser-induced temperature excursions T_1 and T_2, thermal conductivities k_1 and k_2 in layers 1 and 2, respectively. The air thermal conductivity is ignored ($k_0 = 0$). Taking into account NF k anisotropy with the in-plane value k_1 and cross-plane one αk_1, heat conduction equations are:

$$\left(\alpha\frac{\partial^2}{\partial z^2}+\frac{1}{r}\frac{\partial}{\partial r}r\frac{\partial}{\partial r}\right)T_1=-\frac{q_V}{k_1}\quad(0\leqslant z\leqslant h) \tag{3}$$

$$\left(\frac{\partial^2}{\partial z^2}+\frac{1}{r}\frac{\partial}{\partial r}r\frac{\partial}{\partial r}\right)T_2=0\quad(z\geqslant h) \tag{4}$$

Boundary conditions are:

$$\text{for}\quad z=0\quad \frac{\partial T_1}{\partial z}=0; \tag{5}$$

$$\text{for}\quad z=h\quad T_1-T_2=R_K q_S\quad\text{and}\quad q_S=-\alpha k_1\frac{\partial T_1}{\partial z}=-k_2\frac{\partial T_2}{\partial z} \tag{6}$$

$$\text{at}\quad r\to\infty\ T_1=T_2=0;\quad \text{at}\quad z\to\infty\ T_2=0 \tag{7}$$

where q_S is the specific flux density of heat and R_K is the interfacial NF/substrate thermal boundary resistance (Kapitza resistance).

After Hankel transform, we obtain a system of equations that we solve using Green's function method. Finally, we calculate the averaged laser-induced heating ΔT_{calc} of the illuminated area of the layer1.

$$\Delta T_{calc}=\int_{V_1}T_1(\vec{x})q_V(\vec{x})d^3\vec{x}\Big/\int_{V_1}q_V(\vec{x})d^3\vec{x} \tag{8}$$

For solving the inverse problem, we calculated ΔT_{calc} per laser power $\Delta T_{calc}/P$ for a wide range of NF/substrate k ratios k_1/k_2 and compared it with the experimentally determined ratio $\Delta T/P$. k_1 was found from the condition $\Delta T/P = \Delta T_{calc}/P$.

Strictly speaking, the heat conduction Eqs. (3) and (4), assuming diffusive phonon transport (DPT), become incorrect for NFs thinner than the phonon mean free path Λ, which implies mixed diffusive-ballistic phonon transport. However, as was shown for suspended Si NMs with $h < \Lambda$, calculation of the laser-induced temperature field using 2D heat conduction equation gives good results [16,20–22]. Recent Monte Carlo simulations also support validity of the in-plane DPT approach [30].

In an illuminated suspended NM, heat spreads radially from the heated spot to a radius with fixed ambient temperature. In our case of the radially-infinite NF, we expect that the heat conduction Eqs. (3) and (4) also can be used within certain limits. The small but non-zero heat conductivity of the substrate k_2 ($k_1/k_2 \gg 1$) confines the heat in the film, which flows a long distance before it is absorbed in the substrate. Over this large radial distance, DPT dominates over ballistic one and, therefore, description by the heat conduction equation is acceptable. For too small h, our approach is no longer valid due to the significance of the cross-plane ballistic phonon transport. It is important to experimentally examine the limits of validity of the considered theoretical approach.

Calculated temperature fields $T_1(z)$ and $T_1(x)$ for 75 nm thick SOQ (λ = 561 nm, r_0 = 250 nm, P = 1 mW and k_1 = 65.5 W/m/K, the value we explain later) are shown in Fig. 2a (right axis, blue curves) and 2b, respectively. One can see that the temperature is nearly uniform for $T(z)$ with a variation of only ~0.05 K and no noticeable gradients, which can occur at higher Si extinction at shorter λ and cause stress. $T_1(x)$ is slowly decreasing from its maximal value T_{max} at the center of the laser spot to $\sim 0.2T_{max}$ at $x \sim 4500$ nm confirming long-range in-plane heat transport in SOQ. It is remarkable that the influence of either α or R_K on the temperature field is negligible. Indeed, $T_1(z)$ shows only ~0.01 K increase when we introduce largest possible $R_K \sim 4 \times 10^{-9}$ m^2 K/W corresponding to a weak interfacial Si/SiO$_2$ coupling [31]. Introduction of $\alpha = 0.5$ makes negligible changes of the same order in $T_1(z)$. Negligible changes in the temperature field caused by $R_K \sim 4 \times 10^{-9}$ m^2 K/W or $\alpha = 0.5$ cannot be recognized in the $T_1(x)$ dependence (Fig. 2b).

A decade ago, one of the authors of the present work (P. I. Geshev) theoretically considered Gaussian-laser-beam-induced stationary heating of a moving sheet [32]. It was shown that the sheet temperature field displayed a tail in the direction of its movement. With a decrease in the sheet velocity, this tail filled a larger volume. At the zero sheet velocity, there was no stationary solution to the problem. However, as we showed above, a stationary solution exists for a supported sheet even at the zero velocity.

3. Experimental

Raman measurements were performed using a Nanofinder 30 confocal Raman system (Tokyo Instruments Inc.) equipped with 561 nm and 364 nm lasers. Most of measurements were made with a 100× N.A. 0.95 lens and 561 nm laser. The in-plane light intensity distribution was measured while scanning the focused beam across 50 nm × 50 nm Si NW and detecting NW Raman signal (Fig. 1b). Gaussian fitting $\exp(-((X-X_0)/r_0)^2)$ to the obtained curve yields the laser beam radius $r_0 = 249 \pm 2$ nm for the 561 nm light and N.A. 0.95 lens. Measurements with the 364 nm excitation were done with the N.A. 0.5 Mitsutoyo 100× lens displaying $r_0 = 247 \pm 3$ nm. We used the value of $r_0 \sim 250$ nm for both cases.

For SOQ/SOS NFs displaying sharp Raman bands, we employed a 75 g/mm echelle diffraction grating working in the 43rd and 65th orders at the 561 nm and 364 nm excitation wavelengths, respectively. The spectral resolution was ~0.5 cm^{-1}. The experimental error in the Raman peak position was ~0.01 cm^{-1}. For NC Si films displaying relatively broad and weak Raman bands, we used a 1200 g/mm grating with the blazing wavelength of 600 nm and spectral resolution of ~3 cm^{-1} at the 561 nm wavelength. The experimental error in the Raman peak position was ~0.1 cm^{-1}.

A single Raman spectrum measurement of SOQ film took 5–20 s depending on the laser excitation power. For obtaining $\Delta T/P$ slope, 4–5 points were sufficient. The calculation of k using obtained $\Delta T/P$ took about 20 s. Therefore, 5 min was more than enough to obtain

k of one SOQ film. Change of a sample took a few seconds. Therefore, 1 h was enough to get results for a dozen of SOQ films. NC Fe-Si displays a weaker Raman signal, 20–60 s being required to get a spectrum with a good signal/noise ratio. Nevertheless, we were able to examine about 10 samples in 1 h.

Initial commercially available 75 nm thick SOQ NF was received from Shinetsu Co. Then it was thinned via thermal oxidation and etching in HF. Reflection and transmission spectra were used to control both h and absorption of SOQ NFs (Fig. 3).

Composite Fe-Si NC NF was fabricated using phase separation from amorphous Fe–Si alloy film that had a composition ratio of Si/Fe ~ 20 similar to Ni-Si NC NF [11]. The P-doped amorphous Fe-Si alloy film was deposited on quartz by DC magnetron sputtering. To crystallize, the film was annealed at 800 °C for 30 min in N_2. After the crystallization, for the P dopant activation, rapid thermal annealing was performed at 1200 °C with infrared-lamp heating for 10 s in the N_2 ambient. 400 nm thick NC SiGe films were deposited on quartz also using DC magnetron sputtering. After the deposition, the films were annealed at 800 °C for 1 h and 1100 °C for 30 s.

4. Results and discussion

For testing our method of extraction of the film k from the experimental $\Delta T/P$ value, we considered three cases: (1) $h < \Lambda$, $k_1/k_2 \gg 1$; (2) $h < \Lambda$, $k_1/k_2 \sim 1$; (3) $h > \Lambda$, $k_1/k_2 \sim 1$. In the first case, we measured k of Si on quartz (SOQ) NFs. The condition $h < \Lambda$ is satisfied considering that bulk Si has a $\Lambda \sim 300$ nm [33]. 35–75 nm thick Si films display k of several tens of W/m/K, which is significantly larger than the k of quartz ~1.4 W/m/K. Therefore, the condition $k_1/k_2 \gg 1$ is also satisfied. For the second case, we considered 75 nm thick Si on sapphire (SOS). We used directionally averaged value $k_2 = 24$ W/m/K for sapphire. Composite Fe-Si NC NF on quartz with $h \sim 170$ nm > Λ and $k_1/k_2 \sim 1$ corresponds to the third case.

Raman spectra of the 75 nm thick SOQ taken with the 561 nm excitation wavelength at $P \sim 5.5$ mW and ~0.12 mW are shown in Fig. 4. Experimental spectra are shown as open circles while their Lorentzian fittings are displayed as curves. The longitudinal optical phonon Raman band peak positions at ~519.61 cm^{-1} and ~520.41 cm^{-1} are determined with a very high precision of ~0.01 cm^{-1}. This allows utilization of low excitation power and very moderate film heating. The Raman band displays clear down-shift with an increase in the laser power.

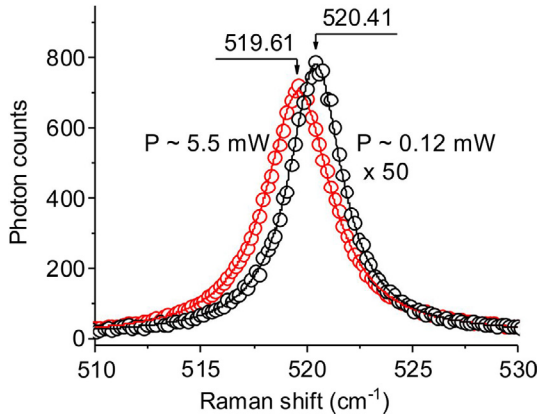

Fig. 4. Raman spectra (circles) and their Lorentz curve fittings of 75 nm thick SOQ for $\lambda = 561$ nm with $P \sim 0.12$ mW (black) and $P \sim 5.5$ mW (red). (For interpretation of the references to color in this figure legend, the reader is referred to the web version of this article.)

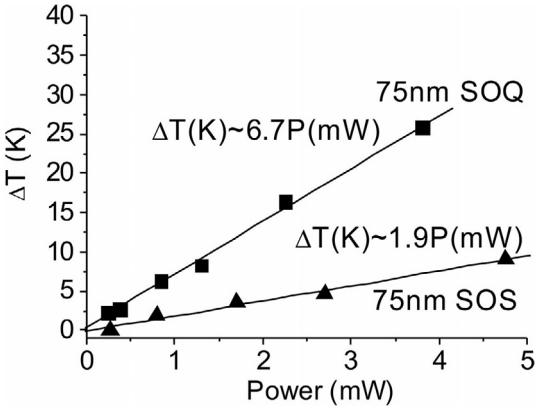

Fig. 5. 75 nm thick SOQ (squares) and SOS (triangles) $\Delta T(P)$ dependencies and their linear fittings.

Fig. 5 shows the laser power dependencies of the laser-induced heating ΔT and their linear fittings for 75 nm thick SOQ and SOS. Inset shows Raman spectra of 75 nm SOQ taken at $P \sim 0.12$ mW and ~5.5 mW. The SOQ dependence is much steeper than the SOS one due to the lesser value of k_2 of quartz compared to sapphire. From the slopes of the dependencies, we find $\Delta T/P \sim 6.7$ (K/mW) for SOQ and $\Delta T/P \sim 1.9$ (K/mW) for SOS. Determination of the corresponding k_1 values is graphically shown in Fig. 6. Straight horizontal lines represent experimental dimensionless $P/\Delta T/\lambda/k_2$ values for the 75 nm thick SOQ and SOS while curves show $P/\Delta T_{calc}/\lambda/k_2$ values calculated for a wide range of k_1/k_2 ratios. The k_1 can be found from their intersection that corresponds to the condition $\Delta T/P = \Delta T_{calc}/P$. The black line intersection point corresponds to $k_1/k_2 \sim 46.8$ i.e. to $k_1 \sim 65.5$ W/m/K for SOQ while the red line intersection point corresponds to $k_1/k_2 \sim 0.92$ i.e. to $k_1 \sim 22$ W/m/K for SOS. The k_1 value obtained for SOQ appears to be in good agreement with literature [34] while that of SOS does not. Therefore, the thickness of 75 nm is sufficient for the heat confinement in Si film on a quartz support while it is not for a sapphire support.

R_K and α impacts on the determined 75 nm thick SOQ k_1 appear to be negligible. $R_K = 4 \times 10^{-9}$ m^2 K/W causes ~0.1 W/m/K increase while $\alpha = 0.5$ causes ~0.03 W/m/K increase in the obtained k_1. R_K and α could be important in the case of SOS when the

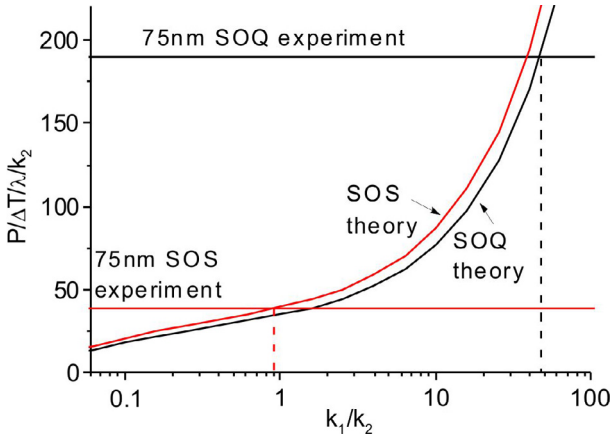

Fig. 6. Dependencies of calculated dimensionless parameter $P/\Delta T_{calc}/\lambda/k_2$ on k_1/k_2 for 75 nm thick SOQ and SOS (black and red curves, respectively). Horizontal lines of corresponding colours represent experimentally determined values of $P/\Delta T/\lambda/k_2$. Vertical dashed lines show the determined k_1/k_2 for both cases. (For interpretation of the references to color in this figure legend, the reader is referred to the web version of this article.)

cross-plane diffusive-ballistic heat transport is significant, e.g. formal utilization of $R_K \sim 3 \times 10^{-8}$ m^2 K/W or $\alpha = 0.02$ for Si/sapphire boundary allows to get agreement between SOS experiment and our theoretical model but this issue requires more detailed study.

Fig. 7 shows the theoretical and experimental Si NF thickness dependencies of k: The theoretical data from literature [34] were obtained assuming in-plane DPT and frequency-dependent boundary scattering. Our experimental data for $\lambda =$ 561 nm (open circles) for SOQ with $h \geq 60$ nm appeared to be in good agreement with theoretical and experimental in-plane Si NF k values from Refs. [34,35]. However, for SOQ with $h < 60$ nm, k_1 rapidly drops with a decrease in h, probably, indicating significance of the cross-plane ballistic phonon transport. In this case like in case of SOS, our theoretical model needs modification.

SOQ k values obtained with the 364 nm laser (Fig. 7, open squares) are overestimated. This is a sequence of a compressive stress caused by the thermal gradient (Fig. 2), which pushes Si Raman shift up while the heating pushes it down. Therefore, the resulting Raman downshift $\Delta\omega$ appears to be smaller and ΔT appears to be lower than it, actually, is. Stress-related errors are discussed in Ref. [36].

Now let us consider the case with $h > \Lambda$ and $k_1/k_2 \sim 1$. Fig. 8 shows the laser power dependencies for 170 nm thick Fe-Si NC NF (black squares) and 400 nm thick $Si_{0.75}Ge_{0.25}$ NC NF (open squares). The dependencies are much steeper than those for SOQ and SOS with $\Delta T/P \sim 87.8$ K/mW and ~134.6 K/mW for Fe-Si NC and SiGe NC films, respectively. Fig. 9 illustrates the k_1 determination for Fe-Si NC NF. The inset shows a TEM image of Fe-Si NC NF cross-section with few tens nanometer grain sizes. In SiGe NC films, the grain sizes were of the same order. Usually, in NC films, Λ is considered to be of the same order as the grain size. However, recently, it was shown that the Λ in NC Si NF is even lower than the grain size [37]. Therefore, probably, Λ is in the range of 20–30 nm in our Fe-Si NC and SiGe NC films satisfying $\Lambda < h$ criterion. Both NFs exhibit low thermal conductivity, namely $k_1 \sim 3.5$ W/m/K for Fe-Si NC NF and $k_1 \sim 2.4$ W/m/K for SiGe NC NF in reasonable agreement with the value obtained using thermal reflectance. Lower k_1 value for SiGe NC NF is, probably, associated with the enhancement of the alloy phonon scattering compared to that in Fe-Si NC NF.

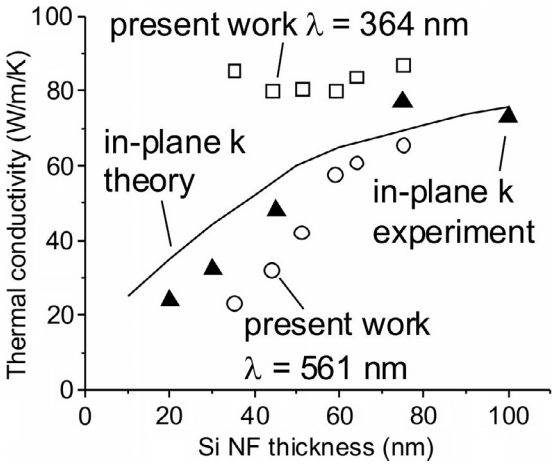

Fig. 7. Thickness dependence of Si NF thermal conductivity k: (1) theoretical and experimental results for in-plane k [34] (black curve and triangles, respectively), and (2) results obtained in this work with $\lambda = 561$ nm (open circles) and 364 nm (open squares).

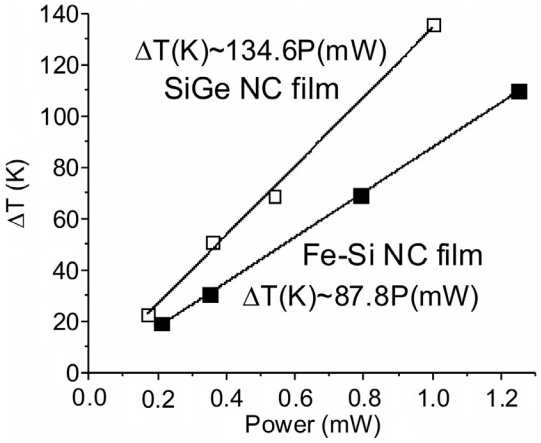

Fig. 8. 170 nm thick Fe-Si NC NF (black squares) and 400 nm thick SiGe NC NF (open squares) ΔT (P) dependencies and their linear fittings.

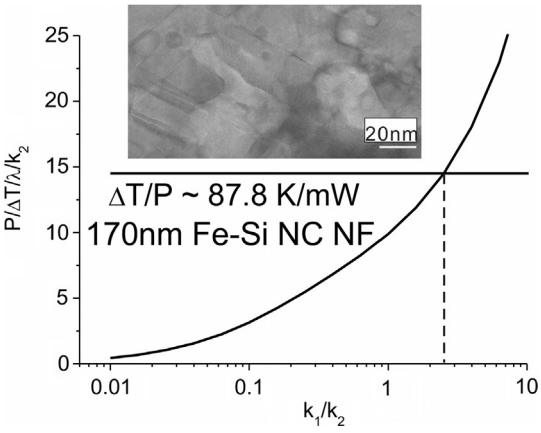

Fig. 9. Dependence of the calculated (curve) dimensionless parameter $P/\Delta T_{calc}/\lambda/k_2$ on k_1/k_2 for 170 nm thick Fe-Si NC NF and experimentally determined value of the parameter $P/\Delta T/\lambda/k_2$ (horizontal line). Vertical dashed line shows the determined k_1/k_2. Inset shows TEM image of Fe-Si NC NF film cross-section.

5. Conclusion

To summarize, using Raman thermometry, we established a simple and efficient method to measure k of absorbing NFs on low-k bulk substrates. The method implies substrate transparency unless NF completely absorbs the light. Assuming DPT, we have calculated the averaged stationary laser-induced NF heating per laser power $\Delta T_{calc}/P$ for a wide range of NF/substrate k ratios k_1/k_2 and compared it with the experimentally determined $\Delta T/P$. Film k was found from the condition $\Delta T/P = \Delta T_{calc}/P$. We applied the method to k measurements of 35–75 nm thick Si NFs ($h < \Lambda$) and nanocomposite 170 nm thick Fe-Si NC and 400 nm thick SiGe NC NFs ($h > \Lambda$) on quartz substrates. As experiments with the nanocomposite NFs show, the method works for relatively thick NFs with $h > \Lambda$, even for $k_1/k_2 \sim 1$ since the DPT dominates. For NFs with $h < \Lambda$ and $k_1/k_2 \gg 1$, the method also works when the NF-confined heat flows a long radial distance before it is absorbed by the substrate, in-plane DPT dominating. We show that the influence of the thermal boundary resistance on the determined k_1 is negligible at this condition. Our experiments show that the method is applicable for Si NFs on quartz substrates for $h \geq 60$ nm suggesting that the DPT dominates in this h range.

A proper choice of the excitation laser wavelength is important. The 561 nm wavelength appeared to be suitable for Si and SiGe due

to the relatively weak absorption and, therefore low thermal gradients. However, the 364 nm wavelength excitation caused stresses in Si-on-quartz because of the high thermal gradients. The stresses did not allow obtaining the correct k values. Some non-thermal photo-induced effects also may cause problems in the k determination but this is not the case for Si and SiGe at λ = 561 nm.

Conflict of interest

We have no conflict of interests.

Acknowledgements

We thank MEXT KAKENHI Grant No 25289200/JSPS, ALCA/JST, Nazarbayev University Grant # SST2015014 and MES RK state-target programs BR05236524 and BR05236454. Geshev thanks support of MES RF. A part of this work was conducted at the AIST Nano-Processing Facility, supported by "Nanotechnology Platform Program" of MEXT, Japan.

References

[1] D. Li, Y. Wu, P. Kim, L. Shi, P. Yang, A. Majumdar, Thermal conductivity of individual silicon nanowires, Appl. Phys. Lett. 83 (2003) 2934–2936.
[2] A.I. Boukai, Y. Bunimovich, J. Tahir-Kheli, J.-K. Yu, W.A. Goddard, J.R. Heath, Si nanowires as efficient thermoelectric materials, Nature 451 (2008) 168–171.
[3] Z. Tian, K. Esfarjani, J. Shiomi, A.S. Henry, G. Chen, On the importance of optical phonons to thermal conductivity in nanostructures, Appl. Phys. Lett. 99 (2011) 053122.
[4] A. Balandin, K.L. Wang, Significant decrease of the lattice thermal conductivity due to phonon confinement in a free-standing semiconductor quantum well, Phys. Rev. B 58 (1998) 1544–1549.
[5] K. Hippalgaonkar, B. Huang, R. Chen, K. Sawyer, P. Ercius, A. Majumdar, Fabrication of microdevices with integrated nanowires for investigating low-dimensional phonon transport, NANO Lett. 10 (2010) 4341–4348.
[6] A.I. Hochbaum, R.K. Chen, R.D. Delgado, W.J. Liang, E.C. Garnett, M. Najarian, A. Majumdar, P.D. Yang, Enhanced thermoelectric performance of rough silicon nanowires, Nature 451 (2008) 163–167.
[7] S. Mukherjee, U. Givan, S. Senz, A. Bergeron, S. Francoeur, M. de la Mata, J. Arbiol, T. Sekiguchi, K.M. Itoh, D. Isheim, D.N. Seidman, O. Moutanabbir, Phonon engineering in isotopically disordered silicon nanowires, NANO Lett. 15 (2015) 3885–3893.
[8] T. Zushi, K. Ohmori, K. Yamada, T. Watanabe, Effect of a SiO_2 layer on the thermal transport properties of (100) Si nanowires: a molecular dynamics study, Phys. Rev. B 91 (2015) 115308.
[9] D.G. Cahill, P.V. Braun, G. Chen, D.R. Clarke, S. Fan, K.E. Goodson, P. Keblinski, W.P. King, G.D. Mahan, A. Majumdar, H.J. Maris, S.R. Phillpot, E. Pop, L. Shi, Nanoscale thermal transport II 2003–2012, Appl. Phys. Rev. 1 (2014) 011305.
[10] S.V. Novikov, A.T. Burkov, J. Schumann, Enhancement of thermoelectric properties in nanocrystalline M-Si thin film composites (M = Cr, Mn), J. Alloys Comp. 557 (2013) 239–243.
[11] N. Uchida, T. Tada, Y. Ohishi, Y. Miyazaki, K. Kurosaki, S. Yamanaka, Heavily doped silicon and nickel silicide nanocrystal composite films with enhanced thermoelectric efficiency, J. Appl. Phys. 114 (2013) 134311.
[12] G.S. Doerk, C. Carraro, R. Maboudian, Temperature dependence of Raman spectra for individual silicon nanowires, Phys Rev. B 80 (2009) 073306.
[13] V. Poborchii, T. Tada, T. Kanayama, Giant heating of Si nanoparticles by weak laser light: optical micro-spectroscopic study and application to particle modification, J. Appl. Phys. 97 (2005) 104323.
[14] B. Stoib, S. Filser, J. Stötzel, A. Greppmair, N. Petermann, H. Wiggers, G. Schierning, M. Stutzmann, M.S. Brandt, Spatially resolved determination of thermal conductivity by Raman spectroscopy, Semicond. Sci. Technol. 29 (2014) 124005.
[15] J. Jaramillo-Fernandez, E. Chavez-Angel, C.M. Sotomayor-Torres, Raman thermometry analysis: modelling assumptions Revisited, Appl. Therm. Eng. 130 (2018) 1175–1181.
[16] E. Chávez-Ángel, J.S. Reparaz, J. Gomis-Bresco, M.R. Wagner, J. Cuffe, B. Graczykowski, A. Shchepetov, H. Jiang, M. Prunnila, J. Ahopelto, F. Alzina, C.M. Sotomayor Torres, Reduction of the thermal conductivity in free-standing silicon nano-membranes investigated by non-invasive Raman thermometry, APL Mater. 2 (2014) 012113.
[17] A.A. Balandin, S. Ghosh, W.Z. Bao, I. Calizo, D. Teweldebrhan, F. Miao, C.N. Lau, Superior thermal conductivity of single layer graphene, Nano Lett. 8 (2008) 902–907.
[18] S. Chen, A.L. Moore, W. Cai, J.W. Suk, J. An, C. Mishra, C. Amos, C.W. Magnuson, J. Kang, L. Shi, R.S. Ruoff, Raman measurement of thermal transport in suspended monolayer graphene of variable sizes in vacuum and gaseous environments, ACS Nano 5 (2010) 321–328.
[19] W. Cai, A.L. Moore, Y. Zhu, X. Li, S. Chen, L. Shi, R.S. Ruoff, Thermal transport in suspended and supported monolayer graphene grown by chemical vapor deposition, Nano Lett. 10 (2010) 1645–1651.
[20] X. Liu, X. Wu, T. Renc, *In situ* and noncontact measurement of silicon membrane thermal conductivity, Appl. Phys. Lett. 98 (2011) 174104.
[21] J.S. Reparaz, E. Chavez-Angel, M.R. Wagner, B. Graczykowski, J. Gomis-Bresco, F. Alzina, C.M. Sotomayor Torres, A novel contactless technique for thermal field mapping and thermal conductivity determination: two-laser Raman thermometry, Rev. Sci. Instrum. 85 (2014) 034901.
[22] B. Graczykowski, A. El Sachat, J.S. Reparaz, M. Sledzinska, M.R. Wagner, E. Chavez-Angel, Y. Wu, S. Volz, Y. Wu, F. Alzina, C.M. Sotomayor Torres, Thermal conductivity and air-mediated losses in periodic porous silicon membranes at high temperatures, Nat. Commun. 8 (2017) 415.
[23] G.S. Doerk, C. Carraro, R. Maboudian, Single nanowire thermal conductivity measurements by Raman thermography, ACS Nano 4 (2010) 4908–4914.
[24] I.-K. Hsu, R. Kumar, A. Bushmaker, S.B. Cronin, M.T. Pettes, Li Shi, T. Brintlinger, M.S. Fuhrer, J. Cumings, Optical measurement of thermal transport in suspended carbon nanotubes, Appl. Phys. Lett. 92 (2008) 063119.
[25] M. Soini, I. Zardo, E. Uccelli, S. Funk, G. Koblmüller, A. Fontcuberta i Morral, G. Abstreiter, Thermal conductivity of GaAs nanowires studied by micro-Raman spectroscopy combined with laser heating, Appl. Phys. Lett. 97 (2010) 263107.
[26] V. Poborchii, Y. Morita, J. Hattori, T. Tada, P.I. Geshev, Corrugated Si nanowires with reduced thermal conductivity for wide-temperature-range thermoelectricity, J. Appl. Phys. 120 (2016) 154304.
[27] S. Xu, T. Wang, D. Hurley, Y. Yue, X. Wang, Development of time-domain differential Raman for transient thermal probing of materials, Opt. Express 23 (2015) 10040–10056.
[28] Landau, Lifshitz, Electrodynamics of Continuous Media, second ed., Pergamon, 1984, p. 273.
[29] V. Poborchii, T. Tada, Y. Morita, S. Migita, T. Kanayama, P.I. Geshev, Enhancement of the ultraviolet absorption and Raman efficiencies of a few nanometer thick Si-on-insulator, J. Appl. Phys. 112 (2012) 074317.
[30] Yu-Chao Hua, Bing-Yang Cao, The effective thermal conductivity of ballistic–diffusive heat conduction in nanostructures with internal heat source, Int. J. Heat Mass Transfer 92 (2016) 995–1003.
[31] J. Chen, G. Zhang, B. Li, Thermal contact resistance across nanoscale silicon dioxide and silicon interface, J. Appl. Phys. 112 (2012) 064319.
[32] R. Brockmann, K. Dickmann, P. Geshev, K.-J. Matthes, Calculation of temperature field in a thin moving sheet heated with laser beam, Int. J. Heat Mass Transfer 46 (2003) 717–723.
[33] Y.S. Ju, K.E. Goodson, Phonon scattering in silicon films with thickness of order 100 nm, Appl. Phys. Lett. 74 (1999) 3005–3007.
[34] C. Jeong, S. Datta, M. Lundstrom, Thermal conductivity of bulk and thin-film silicon: a Landauer approach, J. Appl. Phys 111 (2012) 093708.
[35] W. Liu, M. Asheghi, J. Appl. Phys. 98 (2005) 123523.
[36] T. Beechem, L. Yates, S. Graham, Error and uncertainty in Raman thermal conductivity measurements, Rev. Sci. Instrum. 86 (2015) 041101.
[37] Z. Wang, J.E. Alaniz, W. Jang, J.E. Garay, C. Dames, Thermal conductivity of nanocrystalline silicon: importance of grain size and frequency-dependent mean free paths, NANO Lett. 11 (2011) 2206–2213.